Proton-nucleus total cross sections in the intermediate energy range

L. Ray

Theoretical Division, Los Alamos Scientific Laboratory, University of California, Los Alamos, New Mexico 87545

(Received 16 April 1979; revised manuscript received 20 July 1979)

Proton-nucleus total and reaction cross sections are computed for a number of target nuclei at energies ranging from 100 to 2200 MeV using the Kerman, McManus, and Thaler optical potential formalism and the impulse approximation. Corrections due to Pauli, short-range dynamical, and center-of-mass correlations are included in the calculations. In addition, the electric form factor of the neutron and the nucleon magnetic moments are included in deriving the necessary proton densities from available empirical charge distributions. The proton-nucleon scattering amplitudes are obtained from phase shift solutions or directly from the published N-N data. The proton and neutron point densities are deduced where possible from analyses of electron and proton scattering or from Hartree-Fock predictions if the appropriate elastic angular distribution data are unavailable. An estimate of the uncertainty in the calculated total cross sections is given. The total and reaction cross sections computed in this way are shown to be in very good agreement with the data above 400 MeV but overestimate the data by 15-25% at lower energies, indicating that the approximate multiple scattering calculations generally performed near 1 GeV are inadequate when applied at energies below 400 MeV. Several theoretical improvements are suggested for this lower energy range and some numerical estimates are given. Analysis of total cross section data is also shown to be an unsuitable method for obtaining accurate measurements of neutron matter densities.

[NUCLEAR REACTIONS proton-nucleus scattering; total and reaction cross sections; E_p=100 to 2200 MeV; targets ^{12}C, ^{16}O, ^{27}Al, ^{56}Fe, ^{63,65}Cu, ^{72,74}Ge, ^{127}I, and ^{208}Pb; Kerman, McManus, and Thaler optical potential; target nucleon correlations.]

I. INTRODUCTION

The recent literature in nuclear physics contains many analyses of intermediate energy proton-nucleus elastic scattering data.[1-10] One of the primary goals of these studies is the extraction of neutron density distributions and root-mean-square radii[1-5,9,10] with attention mainly being given to nuclei with $A \geq 12$. Correlation effects,[4-10] electromagnetic corrections,[4] and spin dependence[1-4] have been studied in detail and their effects on the deduced nuclear matter radii assessed. Model-independent analyses[3] have shown which regions of the nuclear density are most sensitively probed by ~1 GeV protons and exhaustive studies of the numerous systematic sources of uncertainty which enter into the numerical analysis of the data have assigned realistic errors to the neutron radii and distributions.[3] What is, of necessity, assumed in all these analyses is that the multiple scattering theories of Kerman, McManus, and Thaler[11] (KMT) or Glauber[12] are correct. More importantly, these analyses assume that the impulse approximation,[11] which is inevitably employed in numerical calculations, is reasonably valid at 800 and 1000 MeV where all studies of nuclei with $A \geq 12$ have been performed to date.[1-10] Clearly, there is a need to test these approximate applications of multiple scattering theory in order to determine the applicable energy range for such numerical analyses and to obtain some estimate of the accuracy of the theoretical calculations.

In a sense, absolute tests of the accuracy of proton-nucleus elastic scattering calculations have been carried out already by comparing the extracted neutron density distributions and radii with Hartree-Fock predictions. The results of many analyses of proton elastic scattering data on nuclei ranging in mass from 12 to 208 and at energies of 800 and 1000 MeV demonstrate that the overall agreement with the theoretical predictions is very good.[1-5,9,10] Obviously, it is quite important to impose energy dependent tests which do not depend on theoretical models for their comparison.

Five possible tests of multiple scattering calculations have previously been proposed.[3] Each test requires a complete knowledge of the two-nucleon amplitudes and involves exhaustive energy dependent studies and error analyses. In three of these tests the theoretical model is required to reproduce the experimental proton-nucleus polarization, the successive maxima-to-minima ratios in the angular distributions, and the proton-nucleus total cross sections. In the fourth test the deduced neutron radii are required to be energy independent. The fifth test demands agreement between neutron densities deduced with protons and that inferred with other strongly interacting probes such as the

pion and the alpha particle.

In this work the ability of the approximate second-order KMT optical potential to reproduce the experimental proton-nucleus total and reaction cross sections from 100 to 2200 MeV is tested. The potential model employed here makes use of the impulse approximation and neglects nonlocality. This total cross section test will be carried out here since: (1) total and reaction cross section data[13-18] offer the only existent proton-nucleus energy dependent data and (2) the prediction of the total and reaction cross sections is not terribly dependent on the assumed matter densities or on details of the N-N amplitudes but depends primarily on the proton-nucleon total cross sections which are quite well known throughout this energy range. Thus, fairly accurate (±2–4 %) predictions of proton-nucleus total cross sections can be made in this energy range, even for nuclei or at energies for which no elastic angular distribution data exist. Specifically, total and reaction cross sections for 100–2200 MeV proton scattering from ^{12}C, ^{16}O, ^{27}Al, ^{56}Fe, ^{63,65}Cu, ^{72,74}Ge, ^{127}I, and ^{208}Pb will be calculated using the second-order KMT optical potential.[4,11] The work presented here compliments the high energy Glauber calculations of neutron-nucleus total cross sections performed by Franco.[19] The recent Glauber model calculations of proton-nucleus total reaction cross sections from 100 MeV to 1 GeV by Ernst[20] will be discussed and compared with the present results.

Based on the good fits obtained to the 800 (Refs. 1–5) and 1000 MeV (Refs. 5–10) proton elastic scattering using either the KMT or Glauber models and the impulse approximation, one would expect that the experimental total cross sections would be well reproduced at these two energies and indeed they are. By calculating total and reaction cross sections over a wide energy range one can examine the possibility that the success of the 800 and 1000 MeV analyses are merely accidental and can also estimate at what other energies one can expect to obtain high quality fits similar to those near 1 GeV.

In Sec. II the details of the second-order KMT optical potential will be given as well as the method used for calculating the uncertainties in the total and reaction cross sections. In Sec. III, the results of the calculations will be given and compared with the data.[13-18] Further theoretical improvements are suggested and some rough numerical estimates of the effects at low energies of two of these additional corrections will be given. A discussion of the value of total cross sections as direct determinants of neutron matter radii will also be given in this section. Finally in Sec. IV the main results will be summarized and conclusions given.

II. SECOND-ORDER KMT CALCULATIONS OF THE TOTAL AND REACTION CROSS SECTIONS

The theoretical model assumed here to describe the proton-nucleus elastic scattering is the optical potential formalism given by Kerman, McManus, and Thaler[11] and by Feshbach *et al.*[21] The optical potential is expressed in a multiple excitation series,[21] the first term of which is proportional to the free N-N scattering amplitude[11,21] (impulse approximation) and the ground state density form factor. The second-order term is proportional to the two-body target nucleon correlation functions, the third-order term is proportional to products of two- and three-body correlation functions, etc.[21,22] The input necessary for second-order calculations are (1) the spin-dependent, nucleon-nucleon amplitudes, (2) the one-body ground state proton and neutron point densities, and (3) two-body target nucleon correlation functions. Each of these ingredients will be discussed below. Following this the calculational details which are needed to compute total and reaction cross sections and the techniques used to estimate the uncertainties in the predicted total cross section values will be discussed.

A. The two-nucleon amplitudes

Unique, nucleon-nucleon phase shift solutions exist for proton incident energies up to about 500 MeV. Assuming the phase shifts of Arndt, Hackman, and Roper[23] (AHR) the Wolfenstein amplitudes[24-26] were generated using the formalism of Stapp *et al.*[26] For spin zero target nuclei only the spin-independent and the spin-orbit amplitudes [i.e., that proportional to $(\vec{\sigma}_p+\vec{\sigma}_j)\cdot\hat{n}$] contribute to the first-order KMT potential term.[27] For the odd mass nuclei considered here the spin-spin and tensor terms of the proton-nucleus optical potential which result from the double-spin-flip nucleon-nucleon amplitudes are neglected. These terms would be weighted by $1/A$ (i.e., 1/27, 1/63, 1/65, and 1/127) relative to the spin-orbit interaction which itself has only a very minute (see below) effect on the predicted total and reaction cross sections. Thus the N-N amplitudes that are used here are[24]

$$t_{pj}(q^2)=t^0_{pj}(q^2)+it^s_{pj}(q^2)(\vec{\sigma}_p+\vec{\sigma}_j)\cdot\hat{n} \qquad (1)$$

where $\hat{n}=(\vec{k}_i\times\vec{k}_f)/|\vec{k}_i\times\vec{k}_f|$ and $j=p$ or n denotes the target nucleon.

For numerical convenience the amplitudes which were generated directly from the AHR phase shifts were approximated by simple parametrized forms

which are often used at higher energies.[1-10,21,22,27] These forms are

$$t^0_{pj}(q^2) = (ik_0\sigma^T_{pj}/4\pi)(1 - i\alpha_{pj})\exp(-B_{pj}q^2)$$

and (2)

$$t^s_{pj}(q^2) = (ik_0\theta_{pj}/4\pi)(1 - i\alpha_{spj})(q^2/4M^2)^{1/2}\exp(-B_{spj}q^2),$$

where k_0 is the nucleon momentum in the two-nucleon center-of-momentum system and M is the nucleon mass. These simple forms reproduce the actual amplitudes reasonably well at momentum transfers less than 1.5–2.0 fm^{-1}. Perfect reproduction could result if α_{pj} and B_{pj} were allowed to be somewhat momentum transfer dependent. In estimating the uncertainty in the predicted total cross sections, allowances for errors in this Gaussian fitting procedure have been included (see Sec. II E). At energies below 500 MeV the real part of t^s_{pj} is dominant and the parameters θ_{pj}, α_{spj}, and B_{spj} were selected to give the best fit to this part of the complex t^s_{pj} amplitude at small momentum transfer ($\lesssim$2 fm^{-1}). Accurate reproduction of the actual spin-orbit amplitude with parametrizations similar to that in Eq. (2) would require a generalization, namely, considerable momentum transfer dependence of θ_{pj} and α_{spj}. The simple form in Eq. (2) is not adequate if one is interested in calculating proton-nucleus polarization[4] but is adequate for total cross section predictions (see Sec. II E). The most important quantities for proton-nucleus total cross section calculations are σ^T_{pp} and σ^T_{pn}, the N-N total cross sections, which are well known (±1–4%) over the energy range considered here.[28-30] The uncertainties in the other parameters, originating from the error in the AHR phase shifts themselves and due to imprecision in the Gaussian fitting procedure, have been included in the error analysis below, but are not very important for total cross section predictions. Finally for $t_{pp}(q^2)$, only the nuclear part of the amplitude is considered.[26] The Coulomb potential will be added to the final KMT optical potential.[11]

At energies greater than 500 MeV insufficient N-N data exist to permit the determination of unique phase shift solutions. At these energies N-N total cross section measurements,[28-30] very forward angle p-p differential cross section data,[31,32] and dispersion relations[33-35] are used to fix σ^T_{pj} and α_{pj} in Eq. (2). The remaining four parameters are determined by fitting the available N-N angular distribution and polarization data from 500 to 2200 MeV.[28,29,36-40]

Finally, because the spin-orbit part of the optical potential is of such minute importance in relation to total cross section predictions, the t^s_{pp} and t^s_{pn} amplitudes have been averaged to yield an N-N spin-orbit amplitude $\bar{t}^s_p(q^2)$ with parameters $\bar{\theta}_p$, $\bar{\alpha}_{sp}$, and $\bar{B}_{sp}$ analogous to those in Eq. (2). The averaging is carried out by assuming $\bar{\theta}_p = (\theta_{pp} + \theta_{pn})/2$, $\bar{\alpha}_{sp} = (\theta_{pp}\alpha_{spp} + \theta_{pn}\alpha_{spn})/(2\bar{\theta}_p)$, and $\bar{B}_{sp} = (B_{spp} + B_{spn})/2$. The values of the N-N parameters used in these calculations are given in Table I at the specific energies considered here.

B. The ground state, one-body densities

The proton and neutron ground state, one-body densities have, where possible, been taken from electron[41-43] and proton scattering analyses,[2-4,44] respectively. For several of the nuclei for which proton total cross section data exist, no electron or proton elastic scattering angular distributions have been measured and for these cases the predictions of Negele's density matrix expansion[45] (DME) code have been used. One should of course be cognizant that the DME calculation assumes the mean field approximation and therefore is most applicable only to closed shell nuclei.[45] The use of these theoretical densities for nuclei with partially filled shells, which is necessitated by the lack of empirical results, is in general questionable. For instance, detailed reproduction of the

TABLE I. The parameters of the N-N amplitudes in Eq. (2) of the text that are assumed in the calculations reported here.

E_{lab} MeV	σ^T_{pp} mb	α_{pp}	B_{pp} fm^2	σ^T_{pn} mb	α_{pn}	B_{pn} fm^2	$\bar{\theta}_p$ mb	$\bar{\alpha}_s$	$\bar{B}_s$ fm^2
100	33.2	1.87	0.66	72.7	1.00	0.36	−35.8	−8.6	0.33
150	26.7	1.53	0.57	50.2	0.96	0.58	−19.3	−13.0	0.23
200	23.6	1.15	0.56	42.0	0.71	0.68	−28.0	−7.8	0.20
325	24.5	0.45	0.26	36.1	0.16	0.36	−34.6	−4.4	0.15
425	27.4	0.47	0.21	33.2	0.25	0.27	−27.3	−4.0	0.11
550	36.9	0.32	0.04	35.5	−0.24	0.085	96.8	0.76	0.35
650	42.3	0.16	0.07	37.7	−0.35	0.09	6.6	10.5	0.30
800	47.3	0.06	0.09	37.9	−0.20	0.12	4.4	15.9	0.23
1000	47.2	−0.09	0.09	39.2	−0.46	0.12	11.2	5.1	0.20
2200	44.7	−0.17	0.12	42.0	−0.50	0.14	7.25	3.9	0.13

isotopic dependence of the rms charge radii for nonclosed shell nuclei is inadequate.[46] However, comparisons of the DME and the empirical charge radii[42] of 17 nuclei from ^{16}O to ^{208}Pb including both those with closed shells and those with partially filled shells, demonstrate that the absolute magnitudes of the theoretical and experimental charge radii typically differ by only ~0.03 fm with the largest difference being 0.06 fm. Uncertainties of this magnitude will be considered in estimating the errors in the predicted total cross sections. While the DME densities may not be completely satisfactory, this is the only readily available model for several of the nuclei for which total cross section data exist.

For ^{12}C, ^{16}O, ^{27}Al, ^{63,65}Cu, ^{56}Fe, and ^{208}Pb empirical charge densities are given in the literature.[41-43] Following Bertozzi *et al.*[47] the point proton matter density is given by

$$\rho_p(x)=\frac{1}{2\pi^2}\int_0^{q_{\max}} j_0(qx)\,\frac{[\tilde{\rho}_{CH}(q^2)-\tilde{\rho}_n^{(1)}(q^2)-\tilde{\rho}_{so}^{(1)}(q^2)]}{\tilde{G}_E^p(q^2)}\,q^2dq\,, \tag{3}$$

where

$$\tilde{\rho}_{CH}(q^2)=4\pi\int_0^\infty x^2 j_0(qx)\rho_{CH}(x)dx\,, \tag{4}$$

$$\tilde{\rho}_n^{(1)}(q^2)=4\pi\tilde{G}_E^N(q^2)\int_0^\infty x^2 j_0(qx)\rho_n(x)dx\,, \tag{5}$$

$$\tilde{\rho}_{so}^{(1)}(q^2)=-(\pi q^2/M^2)\sum_{\substack{i=\text{unfilled}\\ l\ \text{shells}}}(2G_M^i(q^2)-\tilde{G}_E^i(q^2))(j_i^2-l_i^2-s_i^2)\int_0^\infty\frac{j_1(qx_i)}{(qx_i)}\,\rho_{nlj}(x_i)x_i^2dx_i\,. \tag{6}$$

Thus, in general, the experimental charge density is contributed to not only by the proton electric form factor but also by the neutron's electric form factor and by the magnetic moments of both the protons and neutrons. The empirical charge density is denoted by $\rho_{CH}(x)$, the point neutron density by $\rho_n(x)$, and $\rho_{nlj}(x_i)$ is the single nucleon density for the (nlj) shell model level for the ith nucleon. The sum in Eq. (6) includes all protons and neutrons in partially filled l shells since in j-j coupling those nucleons in filled l shells do not make a net contribution to the spin-orbit correction, at least in first order.[47] The quantities j_i^2, l_i^2, and s_i^2 are the eigenvalues of the squares of the total, orbital, and spin angular momentum operators for the ith nucleon. The empirical nucleon magnetic form factors are given by G_M^i ($i=p$ or n),[48] and the $\tilde{G}_E^i$ are related to the empirical nucleon electric form factors, G_E^i,[48] by

$$\tilde{G}_E^i(q^2)=(1-q^2/8M^2)G_E^i(q^2)\,, \tag{7}$$

where both here and in Eq. (6) M is the nucleon mass. The bound state densities, $\rho_{nlj}(x_i)$, are assumed to be the squares of Woods-Saxon eigenstates.[49] The integration cutoff, $q_{\max}$, in Eq. (3) is set equal to the maximum momentum transfer of the best available electron scattering data for a given nucleus.

Polarized proton scattering data of superb quality exist at 800 MeV for ^{12}C, ^{16}O, and ^{208}Pb.[2-4,44] Second-order KMT analyses[4] of these data yield the neutron densities which have been used here. These densities for ^{12}C and ^{208}Pb are very similar to those which result from first-order KMT analyses.[2,3] The neutron density parameters used here for ^{16}O are $w_n=0.12$, $R_n=2.44$ fm, and $Z_n=0.47$ fm,[44] where

$$\rho_n(r)=\rho_{0n}(1+w_n r^2/R_n^2)/[1+\exp((r-R_n)/Z_n)]\,. \tag{8}$$

The point neutron density distributions for ^{27}Al, ^{63,65}Cu, and ^{56}Fe were determined from the calculated DME densities in the following way. First, the empirical proton densities obtained from Eq. (3) were approximated by two-parameter Fermi ($2pF$) densities [Eq. (8) with $w_n=0$] which have the same half-density and root-mean-square radii as the proton density derived from the empirical charge distribution, resulting in the parameters R_p and Z_p analogous to those in Eq. (8). Next the DME proton and neutron densities were similarly fit with $2pF$ forms producing the parameters R_p^{DME}, Z_p^{DME}, R_n^{DME}, and Z_n^{DME}. The parameter values of the neutron densities for ^{27}Al, ^{63,65}Cu, and ^{56}Fe used in the present calculations were then obtained by setting $R_n=R_p(R_n^{DME}/R_p^{DME})$ and $Z_n=Z_p(Z_n^{DME}/Z_p^{DME})$. Thus the DME proton density is scaled to agree with the empirical proton distribution and the relative neutron-proton DME difference is used to obtain the needed neutron density. Such a procedure is motivated by the excellent agreement between the neutron-proton radii differences predicted by the DME code[45] and

TABLE II. The proton and neutron point density radius and diffuseness parameters obtained from DME predictions as explained in the text.

Nucleus	R_p fm	Z_p fm	R_n fm	Z_n fm
^{27}Al	...	...	3.15	0.46
^{56}Fe	...	...	4.13	0.49
^{63}Cu	...	...	4.20	0.57
^{65}Cu	...	...	4.32	0.56
^{72}Ge	4.35	0.58	4.51	0.56
^{74}Ge	4.36	0.58	4.59	0.56
^{127}I	5.58	0.50	5.61	0.58

that deduced from proton scattering analyses.[1-4] This general theoretical and experimental concordance occurs for both closed and nonclosed shell nuclei.[1-4] Finally the proton and neutron densities for ^{72,74}Ge and ^{127}I have relied solely on $2pF$ fits to the DME predictions, since no electron or proton elastic cross sections are available for these nuclei. Such usage of the DME predictions for nonclosed shell nuclei relies heavily on the ~0.03 fm accuracy discussed above. Table II displays the radius and diffuseness parameters assumed in these calculations for ^{27}Al, ^{63,65}Cu, ^{56}Fe, ^{72,74}Ge, and ^{127}I.

C. The second-order KMT optical potential

A great deal of effort has been expended in the last several years in an effort to calculate approximations to the second-order KMT optical potential.[4,6-9,11,21,22,27] Applications to nuclei with $A \geq 12$ have been given by Harrington and Varma,[6] Layly and Schaeffer,[8] and Boridy and Feshbach.[7] In the KMT formulation the second-order optical potential terms are proportional to the two-body correlation functions. The general effect that these second-order terms have is to increase the diffractive maxima in the elastic angular distribution by 10–30 %. All of these calculations demonstrate that Pauli correlations dominate the second-order corrections and that short-range dynamical correlations and the center-of-mass correlation correction[8,9] are of lesser importance. Since all of these effects are fairly small, Harrington and Varma[6] and Layly and Schaeffer[8] have derived local $\sim\rho^2$ forms for these corrections, the former within the Glauber formalism and the latter using KMT. Both make use of the eikonal approximation.[12] In this and in a previous work[4] the Glauber derivation of Harrington and Varma[6] is used to obtain an approximate ρ^2 form for the second-order optical potential, which when added to the usual first-order optical potential[50] and inserted into the Schrödinger equation, yields the proton-nucleus scattering amplitude.

The purpose of the calculations presented here is to test the accuracy of the total cross section predictions of the approximate KMT calculations which have been applied at ~1 GeV and to determine a low energy limit to such analyses. If one were interested in improving the predictions at lower energies than a number of the simplifications assumed here would become invalid. For instance, the assumption here of local potentials is probably not very good for low energies (~100 MeV) according to the work of Mulligan[51] and Johnson and Martin[52] for the first- and second-order optical potentials, respectively. Many other corrections could also become important at energies near 100 MeV and some of these will be mentioned in Sec. III.

The derivation of Harrington and Varma[6] exploits the eikonal relation between the phase shift and the optical potential. This relationship is given by the integrals[12]

$$\hat{\chi}_{\rm opt}(b) = -\frac{\mu c^2}{\hbar^2 c^2 k_N}\int_{-\infty}^{\infty} dZ\, U^{\rm opt}_{\rm KMT}(r) \tag{9}$$

and

$$U^{\rm opt}_{\rm KMT}(r) = \frac{\hbar^2 c^2 k_N}{\mu c^2 \pi}\,\frac{1}{r}\,\frac{d}{dr}\int_r^{\infty}\frac{\hat{\chi}_{\rm opt}(b)\,b\,db}{(b^2-r^2)^{1/2}}\,. \tag{10}$$

Relativistic kinematics are assumed here, where k_N is the relativistic momentum in the proton-nucleus center-of-momentum system and $\mu c^2 = \epsilon_1\epsilon_2/(\epsilon_1+\epsilon_2)$, ϵ_i being the total relativistic energy of either the incident proton or target nucleus in the proton-nucleus center-of-momentum system.[3,4] The optical phase shift is expanded as $\hat{\chi}_{\rm opt} = \hat{\chi}_1 + \hat{\chi}_2 + \cdots$, where

$$i\hat{\chi}_1(b) = -(A-1)\langle\gamma\rangle \tag{11}$$

and

$$i\hat{\chi}_2(b) = \tfrac{1}{2}(A-1)^2\{\langle\gamma_1\gamma_2\rangle - \langle\gamma\rangle^2\}, \tag{12}$$

and where

$$\langle\gamma\rangle = \int d^3r_1\rho_1(\vec{r}_1)\gamma(\vec{b}-\vec{b}_1) \tag{13}$$

and

$$\{\langle\gamma_1\gamma_2\rangle - \langle\gamma\rangle^2\} = \int\int d^3r_1 d^3r_2 C_2(\vec{r}_1,\vec{r}_2) \times\gamma(\vec{b}-\vec{b}_1)\gamma(\vec{b}-\vec{b}_2)\,. \tag{14}$$

In these expressions ρ_1 is the one-body density, $C_2(\vec{r}_1,\vec{r}_2)$ is the two-body correlation function, and $\gamma(\vec{b})$ is

$$\gamma(\vec{b}) = \frac{1}{2\pi i k_0}\int d^2q\, e^{i\vec{q}\cdot\vec{b}} f(q^2)\,, \tag{15}$$

$f(q^2)$ being the spin-independent part of the N-N scattering amplitude.

Equations (10), (11), (13), and (15) can be used to generate the usual first-order KMT optical potential. To obtain an approximation for the second-order KMT optical potential one needs a model for the two-body correlation functions. Following Boridy and Feshbach, $C_2(\vec{r}_1,\vec{r}_2)$ is expressed as[7]

$$C_2(\vec{r}_1,\vec{r}_2) \cong \rho_1(\vec{r}_1)\rho_1(\vec{r}_2)\{f_{\text{Pauli}}(|\vec{r}_1-\vec{r}_2|)+f_{\text{SRD}}(|\vec{r}_1-\vec{r}_2|) + f_{\text{Pauli}}(|\vec{r}_1-\vec{r}_2|)f_{\text{SRD}}(|\vec{r}_1-\vec{r}_2|)\}. \quad (16)$$

For a noninteracting Fermi gas the Pauli correlation function for a nucleus with A nucleons is[7,53]

$$f_{\text{Pauli}}(x) = -\frac{9}{4}\frac{A-4}{A-1}\left[\frac{j_1(k_F x)}{(k_F x)}\right]^2, \quad (17)$$

where k_F is the local Fermi momentum, here assumed to be position dependent according to[6]

$$k_F(r) = \{1.5\pi^2 A\rho_1(r)\}^{1/3}. \quad (18)$$

The short-range dynamical correlation is assumed to be[7]

$$f_{\text{SRD}}(x) = -\exp(-x^2/b^2) \quad (19)$$

with $b = 0.4$ fm. To enable the six-dimensional integration in Eq. (14) to be carried out analytically, $f_{\text{Pauli}}(x)$ must be approximated by a Gaussian. The best such approximation to Eq. (17) is given by[4,6]

$$f_{\text{Pauli}}(x) \cong -0.3(\pi/5)^{1/2} \times((A-4)/(A-1))\exp(-k_F{}^2x^2/5). \quad (20)$$

Using Eqs. (10), (12), (14), (15), (2), (16), (18), (19), and (20) and replacing $\rho_1(\vec{r}_1)\rho_1(\vec{r}_2)$ with $\rho_1{}^2((\vec{r}_1+\vec{r}_2)/2)$ and assuming that the ranges of the interaction and correlation functions are small compared to the nuclear size, one obtains a simple expression for the second-order optical potential. Three terms arise, corresponding to the three terms in Eq. (16). They are[4]

$$U^{(2)\text{opt}}_{\text{Pauli}}(r) \cong -\frac{i(\hbar c)^2 k_N}{2\mu c^2}(A-1)(A-4)(\hat{\sigma}/2)^2\rho_1{}^2(r) \times[3\pi/(10k_F(r))](1+8Bk_F{}^2(r)/5)^{-1}, \quad (21)$$

$$U^{(2)\text{opt}}_{\text{SRD}}(r) \cong -\frac{i(\hbar c)^2 k_N}{2\mu c^2}(A-1)^2(\hat{\sigma}/2)^2\sqrt{\pi}\rho_1{}^2(r)\frac{b^3}{b^2+8B}, \quad (22)$$

and

$$U^{(2)\text{opt}}_{\text{PSR-I}}(r) \cong \frac{i(\hbar c)^2 k_N}{2\mu c^2}(A-1)(A-4)(\hat{\sigma}/2)^2(3\pi/10)\rho_1{}^2(r) \times[k_F{}^2(r)+5b^{-2}]^{-1/2}\{1+8B[k_F{}^2(r)/5+b^{-2}]\}^{-1}. \quad (23)$$

In these equations $\hat{\sigma}$ and B are defined by,

$$\hat{\sigma} = \bar{\sigma}^T(1-i\bar{\alpha}), \quad (24)$$

and

$$\bar{\sigma}^T = \frac{Z}{A}\sigma^T_{pp}+\frac{N}{A}\sigma^T_{pn}, \quad (25)$$

$$\bar{\alpha} = \frac{Z\sigma^T_{pp}\alpha_{pp}+N\sigma^T_{pn}\alpha_{pn}}{Z\sigma^T_{pp}+N\sigma^T_{pn}}, \quad (26)$$

and

$$B = \frac{Z}{A}B_{pp}+\frac{N}{A}B_{pn}. \quad (27)$$

The density $\rho_1(r)$ is the total matter density normalized such that $\int d^3r\rho_1(r) = 1$.

Layly and Schaeffer[8] have shown that the second-order optical potential can in general be reduced to a simple local form by making the eikonal approximation in the propagator and also the local density approximation. The result is

$$U^{(2)}(q) \cong i(A-1)^2\frac{\mu c^2}{(\hbar c)^2 k_N}t^2(q/2)l_c \times\int e^{-i\vec{q}\cdot\vec{r}'}\rho_1{}^2(\vec{r}')d^3r', \quad (28)$$

where t is the N-N t matrix and l_c is an effective "correlation length." Setting $l_c \cong R_{\text{c.m.}}/A$ and $R_{\text{c.m.}} = (\pi RZ)^{1/2}$, Eq. (28) can be used to estimate the center-of-mass correction.[8,9] In these relations R and Z are the radius and diffuseness of a Fermi matter density. Using Eq. (2)

$$t^2(q/2) = -(\hat{\sigma}/2)^2\left[\frac{(\hbar c)^2 k_N}{\mu c^2}\right]^2\exp(-Bq^2/2), \quad (29)$$

and if one further assumes that the range of the interaction is small compared to the nuclear radius, the second-order optical potential correction due to the center-of-mass correlation is[4,8,9]

$$U^{(2)\text{opt}}_{\text{c.m.}}(r) \cong -i(A-1)^2\left[\frac{(\hbar c)^2 k_N}{\mu c^2}\right](\hat{\sigma}/2)^2(R_{\text{c.m.}}/A)\rho_1{}^2(r). \quad (30)$$

As in Ref. 4 the Pauli correlation correction to the spin-orbit part of the optical potential can be estimated by generalizing the $f(q^2)$ in Eq. (15) to $f_{pj}(q^2) = t^0_{pj}(q^2)+it^s_{pj}(q^2)(\vec{\sigma}_p+\vec{\sigma}_j)\cdot\hat{n}$ as in Eq. (1). Invoking the same approximations and assumptions as above the resulting correction to the spin-orbit potential is[4]

$$U^{(2)\mathrm{opt}}_{\mathrm{Pauli,SO}}(r) \cong -i(A-1)(A-4)(3\pi/1280)\left[\frac{(\hbar c)^3\hat{\theta}\hat{\sigma}}{\mu c^2 \overline{B}_{sp} B M c^2}\right] \times \rho_1(r)\frac{1}{r}\frac{d}{dr}\frac{\rho_1(r)}{k_F(r)\left[\left(\frac{1}{4B}+k_F^2(r)/5\right)\left(\frac{1}{4\overline{B}_{sp}}+k_F^2(r)/5\right)-k_F^4(r)/25\right]}(\vec{\sigma}\cdot\vec{l}), \tag{31}$$

where $\hat{\theta}=\overline{\theta}_p(1-i\overline{\alpha}_{sp})$.

To reiterate, the approximations or assumptions made in obtaining these local $\sim\rho^2$ estimates of contributions to the second-order optical potential are: (1) the eikonal approximation, (2) the local-density approximation, (3) further approximation of the two-nucleon scattering amplitudes and correlation functions with Gaussian forms, and (4) the assumption that the ranges of the N-N interaction and correlation lengths are small compared to the nuclear radius.

Thus, the final complete optical potential used in the calculations reported here is

$$U^{(1+2)\mathrm{opt}}(r)=U^{(1)}(r)+U^{(2)\mathrm{opt}}_{\mathrm{Pauli}}(r)+U^{(2)\mathrm{opt}}_{\mathrm{SRD}}(r)+U^{(2)\mathrm{opt}}_{\mathrm{FSR-I}}(r)+U^{(2)\mathrm{opt}}_{\mathrm{c.m.}}(r)+U^{(2)\mathrm{opt}}_{\mathrm{Pauli,SO}}(r)+U_{\mathrm{Coul}}(r), \tag{32}$$

where $U^{(1)}(r)$ is the usual first-order, spin-dependent KMT optical potential given in detail in Ref. 50, and is basically of the $(A-1)t(q^2)\tilde{\rho}(q^2)$ form[21] and $U_{\mathrm{Coul}}(r)$ is the Coulomb potential for an extended nuclear charge density, $\rho_{\mathrm{CH}}(r)$. The full potential, $U^{(1+2)\mathrm{opt}}(r)$ is then inserted into the Schrödinger equation with relativistic kinematics[3,4] from which the proton-nucleus scattering amplitude is obtained. The radial forms of each term in Eq. (32) are given in Figs. 1 and 2 for the first- and second-order terms, respectively, in relation to the nuclear matter density, $\rho_m(r)=\rho_p(r)+\rho_n(r)$. The typical case shown is for $p+{}^{56}$Fe at 1 GeV.

D. Calculation of total and reaction cross sections for charged particles

The calculation and measurement of total and reaction cross sections for charged particles are complicated by the fact that Coulomb total cross sections are infinite and therefore careful subtractions must be made in order to extract useful

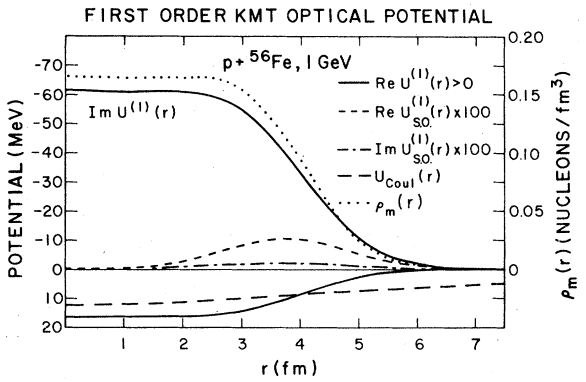

FIG. 1. The radial distributions of the first-order KMT optical potential terms for $p+{}^{56}$Fe at 1 GeV. The real and imaginary parts of the central, spin-independent term are given by the positive and negative solid curves, respectively. The real and imaginary parts of the spin-orbit potential are displayed by the short dashed and dash-dot curves, respectively, where the full spin-orbit term in the Schrödinger equation is written as $U^{(1)}_{\mathrm{so}}(r)\vec{\sigma}\cdot\vec{l}$. Note that the spin-orbit potential has been multiplied by 100 and that no adjustment has been made to fit proton-nucleus analyzing power data. The long dashed curve denotes the Coulomb potential and the dotted line indicates the assumed ^{56}Fe point matter density.

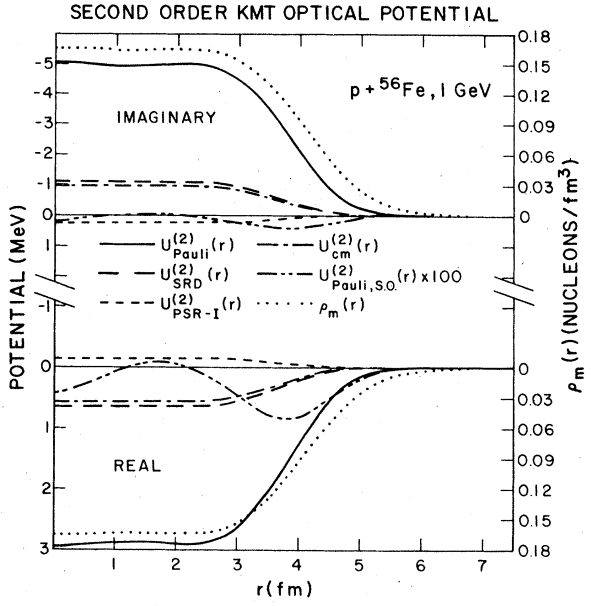

FIG. 2. The radial distributions of the second-order terms of the 1 GeV, $p+{}^{56}$Fe KMT optical potential [see Eq. (32)]. The forms of Eqs. (21), (22), (23), (30), and (31) of the text are indicated by the solid, long dashed, short dashed, dash-dot, and dash-double-dot curves, respectively. The assumed ^{56}Fe point matter density is displayed by the dotted lines. The spin-orbit correction shown here has been multiplied by 100 and does not include the $(\vec{\sigma}\cdot\vec{l})$ factor in Eq. (31).

quantities.[13-18] The expression for the total and reaction cross sections for spin 0 charged particles has been given by Cooper and Johnson.[54] The equations given below follow directly from Ref. 54 with suitable generalization for spin $\frac{1}{2}$ projectiles having been made.

The elastic differential cross section for the scattering of a spin $\frac{1}{2}$ charged projectile from a spin 0 target is[55]

$$d\sigma/d\Omega = |A|^2 + |B|^2 , \tag{33}$$

where

$$A(\theta) = f_c(\theta) + f_N(\theta) \tag{34}$$

and where $f_c(\theta)$ is the Rutherford amplitude[55] and

$$f_N(\theta) = (i/k_N)(A/(A-1)) \sum_l \exp(2i\sigma_l)\{(l+1)\beta_{l,l+1/2} + l\beta_{l,l-1/2}\}P_l(\cos\theta) . \tag{35}$$

The spin-dependent amplitude is given by

$$B(\theta) = (i/k_N)(A/(A-1)) \sum_l \exp(2i\sigma_l)\{\beta_{l,l+1/2} - \beta_{l,l-1/2}\}P_l'(\cos\theta) . \tag{36}$$

The Coulomb phase shift is denoted by σ_l and $\beta_{l,l\pm1/2}$ are obtained from the asymptotic phase shifts which result from the usual matching conditions for the distorted waves generated with the Schrödinger equation and the KMT optical potential in Eq. (32). The $A/(A-1)$ factor in Eqs. (35) and (36) is required by the KMT formalism.[11] Hence the elastic differential cross section is

$$d\sigma/d\Omega = |f_c|^2 + |f_N|^2 + 2\,\mathrm{Re}\{f_c^* f_N\} + |B|^2 . \tag{37}$$

The total proton-nucleus scattering amplitude is[55]

$$f(\theta) = f_c(\theta) + f_N(\theta) + iB(\theta)\vec{\sigma}\cdot\hat{n} , \tag{38}$$

and from the optical theorem[55]

$$\sigma_{\mathrm{TOTAL}} = (4\pi/k_N)\,\mathrm{Im}f_c(0) + (4\pi/k_N)\,\mathrm{Im}f_N(0) \tag{39}$$

because $B(0)=0$. From the definition $\sigma_{\mathrm{TOTAL}} \equiv \sigma_{\mathrm{ELAS}} + \sigma_{\mathrm{REAC}}$ one gets

$$\sigma_{\mathrm{REAC}} = (4\pi/k_N)\,\mathrm{Im}f_c(0) + (4\pi/k_N)\,\mathrm{Im}f_N(0) - 2\pi\int_0^\pi (d\sigma/d\Omega)\sin\theta\, d\theta$$

$$= (4\pi/k_N)\,\mathrm{Im}f_c(0) + (4\pi/k_N)\,\mathrm{Im}f_N(0) - 2\pi\int_0^\pi |f_c|^2 \sin\theta\, d\theta - 2\pi\int_0^\pi \{(d\sigma/d\Omega) - |f_c|^2\}\sin\theta\, d\theta , \tag{40}$$

$$\sigma_{\mathrm{REAC}} = (4\pi/k_N)\,\mathrm{Im}f_N(0) - 2\pi\int_0^\pi \{(d\sigma/d\Omega) - |f_c|^2\}\sin\theta\, d\theta . \tag{41}$$

The last step follows from the optical theorem for potential scattering.[54,55] From Eqs. (37) and (41)

$$\sigma_{\mathrm{REAC}} = (4\pi/k_N)\,\mathrm{Im}f_N(0) - 2\pi\int_0^\pi \{|f_N|^2 + 2\,\mathrm{Re}\{f_c^* f_N\} + |B|^2\}\sin\theta\, d\theta . \tag{42}$$

As in Ref. 54, one defines

$$\tilde{f}_N(\theta) = (i/k_N)(A/(A-1)) \sum_l \{(l+1)\beta_{l,l+1/2} + l\beta_{l,l-1/2}\}P_l(\cos\theta) , \tag{43}$$

and it easily follows that[54]

$$4\pi\int_0^\pi \mathrm{Re}\{f_c^* f_N\}\sin\theta\, d\theta = (4\pi/k_N)\,\mathrm{Im}\{f_N(0) - \tilde{f}_N(0)\} . \tag{44}$$

The total reaction cross section is finally written as

$$\sigma_{\mathrm{REAC}} = (4\pi/k_N)\,\mathrm{Im}\tilde{f}_N(0) - 2\pi\int_0^\pi \{|f_N|^2 + |B|^2\}\sin\theta\, d\theta \tag{45}$$

and the total cross section is given by

$$\sigma_{\mathrm{TOTAL}} = (4\pi/k_N)\,\mathrm{Im}\tilde{f}_N(0) . \tag{46}$$

The expressions in Eqs. (45) and (46) are the quan-

tities which are calculated here and correspond physically to the measurements made in Refs. 13–18.

E. Error analysis

The goal of the calculations presented here is to determine how accurately the total and reaction cross sections are predicted by the optical potential in Eq. (32), which is commonly used in the analysis of ~1 GeV proton elastic scattering data. If discrepancies between the theoretical predictions and the data occur one must know the uncertainty not only in the experimental quantities but also in the theoretical predictions in order to assess the significance of such discrepancies. Since experimental N-N amplitudes and densities are input into the calculations and because they have associated errors,[3] some uncertainty in the predicted total and reaction cross sections arises. The change in σ_{TOTAL} and σ_{REAC} due to the separate variation of each specific input parameter is the basis for the error analysis presented here.

A detailed study of the accuracy of an analysis requires that the correlations between the various input parameters be considered and that the full error matrix[56] be computed. In the error analysis presented here, all uncertainties in the input parameters are assumed to be independent and the individual contributions to the error in the computed total cross sections are added incoherently. Thus the error analyses given here and in Ref. 3 provide a qualitative estimate of the total error and probably overestimate somewhat the total error which would be computed by considering the correlations between parameters.

The uncertainties in the N-N total cross sections and in the real-to-imaginary ratios, α_{pj}, have been taken from the literature.[28-35] The uncertainties in B_{pj}, $\bar{\theta}_p$, $\bar{\alpha}_{sp}$, and $\bar{B}_{sp}$ arise from the variation allowed in fitting the Gaussian forms in Eq. (2) to the N-N data or the scattering amplitudes generated from the AHR N-N phase shifts.[23] The uncertainties in the proton densities are assumed to be the same as that in the charge densities which are taken from the literature.[41-43] The error in the neutron densities deduced from polarized proton scattering analyses at ~1 GeV is estimated in Ref. 3. The total uncertainties in $\langle r_n^2\rangle^{1/2}$ and $\langle r_n^4\rangle^{1/4}$, the second and fourth moments of the neutron distributions, are ±0.07, 0.10 fm, respectively.[3] The neutron radius and diffuseness parameters have been simultaneously varied (typically $\Delta R_n \cong \mp 0.02$ fm while $\Delta Z_n \cong \pm 0.03$ fm) such that $\langle r_n^2\rangle^{1/2}$ and $\langle r_n^4\rangle^{1/4}$ change by these amounts. The resulting changes in the total cross sections are taken to be the error in σ_{TOTAL} and σ_{REAC} owing to the uncertainty in the neutron densities. For nuclei other than ^{12}C, ^{16}O, and ^{208}Pb this same procedure is assumed since the moments of the DME and the empirically deduced neutron densities usually agree to within these amounts.[1-4]

The reader will notice in Refs. 3 and 57 that in a few cases (^{40,48}Ca, ^{124}Sn, and ^{208}Pb) the KMT calculations fail to fit the very forward angle elastic cross section data. For the worst of these cases, ^{40}Ca, the cross section data have recently been retaken, with the new forward angle data being completely consistent with the calculation.[58] For the remaining three cases, no KMT or phenomenological optical model calculation can be found which will simultaneously fit the very forward angle data as well as the remaining diffractive structure. Since these forward angle discrepancies are *not* a general feature at 800 MeV (good

TABLE III. Total cross section uncertainties.[a]

	325 MeV			1000 MeV		
Error source	^{16}O $\Delta\sigma_{tot}$ %	^{63}Cu $\Delta\sigma_{reac}$ %	^{208}Pb $\Delta\sigma_{reac}$ %	^{16}O $\Delta\sigma_{tot}$ %	^{63}Cu $\Delta\sigma_{reac}$ %	^{208}Pb $\Delta\sigma_{reac}$ %
$\Delta\rho_p$	0.10	0.18	0.05	0.31	0.29	0.07
$\Delta\sigma_{pp}$	1.4	0.63	0.31	0.73	0.32	0.15
$\Delta\sigma_{pn}$	1.2	0.73	0.57	0.79	0.39	0.35
ΔB_{pp}	0.30	0.61	0.41	0.04	0.08	0.05
ΔB_{pn}	0.38	0.73	0.64	0.15	0.30	0.25
$\Delta\alpha_{pp}$	1.0	0.13	0.13	0.61	0.18	0.12
$\Delta\alpha_{pn}$	2.2	0.29	0.43	0.65	0.31	0.29
$\Delta(\bar{\theta}_p, \bar{\alpha}_s)$	0.13	0.13	0.07	0.04	0.01	0.01
$\Delta\bar{B}_s$	0.05	0.00	0.00	0.00	0.00	0.00
$\Delta\rho_n$	0.36	1.15	1.48	0.60	1.33	1.62
ΔCorr	0.55	0.19	0.11	0.90	0.18	0.10
Total	3.7	2.0	1.9	2.5	1.7	1.8

[a]All uncertainties given here are ± values in percent.

fits at forward angles are obtained at 800 MeV for 12 other nuclei[1-3,57,59]) and owing to the experimental difficulties which are present in this angular range, as in the ^{40}Ca case,[58] the forward angle data for these few exceptional cases have been omitted from the error analysis of Ref. 3 and are not included in the present error analysis.

In Table III some typical results of this error analysis are presented. The cases shown are for ^{16}O, ^{63}Cu, and ^{208}Pb at 325 and 1000 MeV. The values given in this table are the percentage change in σ_{TOTAL} or σ_{REAC} due to the separate variation of each input parameter listed. The uncertainty in the estimate of the correlation correction is assumed to be ±20% of the full correlation effect. This value is arrived at by comparing the correlation size effects calculated in Refs. 4, 6, 7, and 9, each of which agree to within ~20%. This correlation error estimate is added linearly to the first ten errors in Table III which are added quadratically to give the total uncertainty in the predicted values of σ_{TOTAL} and σ_{REAC}. The average uncertainty in σ_{TOTAL} is ±3.0% and in σ_{REAC} it is about ±2.0%. The largest sources of uncertainty are σ_{pj}^{T}, α_{pj}, B_{pj}, and the neutron densities. In general the total percentage uncertainties decrease slightly with increasing energy and with increasing target mass. Explicit calculations were carried out for ^{16}O, ^{63}Cu, and ^{208}Pb at 100, 325, 650, and 1000 MeV. The total uncertainties at the remaining energies and for the remaining nuclei were estimated by interpolating the explicitly calculated errors.

The actual estimated error in the total reaction cross section decreases only moderately with increasing proton energy, the uncertainty at 1 GeV being about 30% less than that at 100 MeV. The principal contributors to the error in σ_{REAC} are σ_{pj}^{T}, B_{pj}, and the neutron densities. As the energy increases from 100 MeV to 1 GeV the uncertainty in σ_{pj}^{T} and B_{pj} decreases by a factor of 2 or greater and this is reflected in reduced contributions to the uncertainty in σ_{REAC}. The error due to uncertainties in the neutron densities is relatively energy independent, hence the total error in σ_{REAC} decreases by only ~30% as the proton energy is increased to 1 GeV.

III. DISCUSSION OF THE RESULTS

Predictions of σ_{TOTAL} for ^{12}C and ^{16}O and of σ_{REAC} for ^{12}C, ^{16}O, ^{27}Al, ^{63,65}Cu, ^{56}Fe, ^{72,74}Ge, ^{127}I, and ^{208}Pb are shown in Figs. 3–5 in comparison with the published data.[13-18] The Cu and Ge targets used in the measurements of Ref. 14 are of natural composition and σ_{REAC} for ^{63,65}Cu and for ^{72,74}Ge have been appropriately weighted to give atomic masses equal to that quoted for the Cu and Ge targets in Ref. 14. The shaded bands are the results of the second-order KMT optical potential predictions, the widths of the bands being determined by the error analysis in the preceding section. The calculations were performed at energies of 100, 150, 200, 325, 425, 550, 650, 800, 1000, and 2200 MeV. The results shown by the crosshatched regions are qualitatively similar to the Glauber model estimates in Ref. 13. However, the general description of the data in the high energy region (400–2200 MeV) is more satisfactory here than in Ref. 13. Note that σ_{TOTAL} and σ_{REAC} are plotted on an expanded and shifted ordinate so that the data, the theoretical predictions, and the discrepancies between the two are magnified.

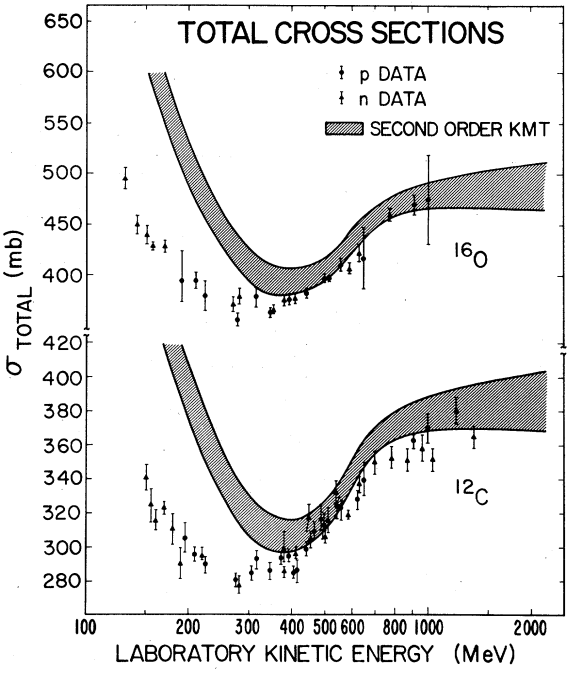

FIG. 3. Proton-nucleus total cross sections for ^{12}C and ^{16}O computed using the second-order KMT optical potential, Eq. (32), and the errors discussed in the text (shaded band). Note that both proton-nucleus (circular points) and neutron-nucleus (triangular points) experimental data are shown here.

The most striking result to be seen in Fig. 3 is the excellent agreement with the data at energies above 400 MeV and the overestimate of the total cross sections below this energy. The overestimate of σ_{TOTAL} is ~25% at 200 MeV. In Figs. 4 and 5 it is seen that general agreement with the data occurs at energies above 350 to 400 MeV and below this the overestimate of σ_{REAC} is ~15% at 200 MeV. The errors and the scatter in the σ_{TOTAL} data[13] for ^{12}C and ^{16}O are about the same size as the un-

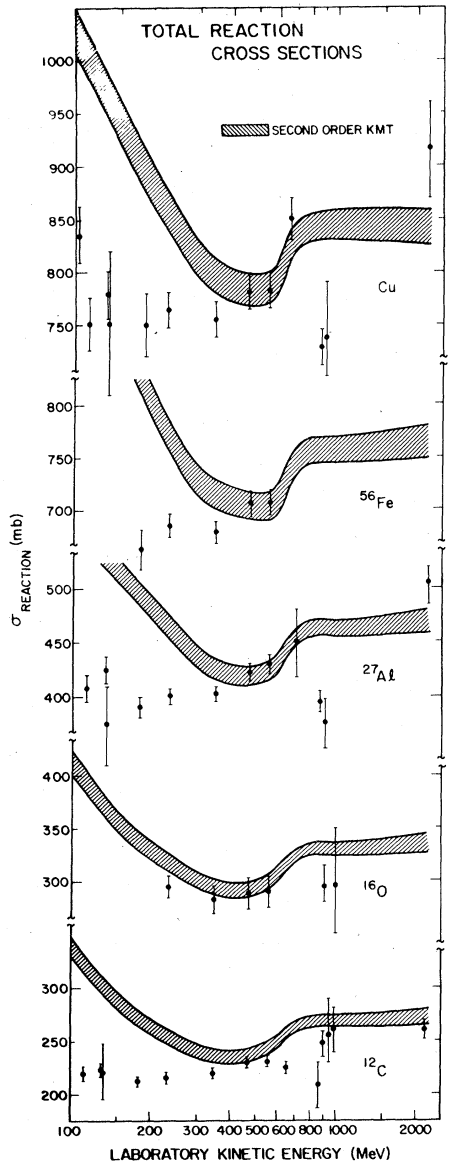

FIG. 4. Proton-nucleus total reaction cross sections for ^{12}C, ^{16}O, ^{27}Al, ^{56}Fe, and Cu predicted by second-order KMT (shaded band) and compared with experiment.

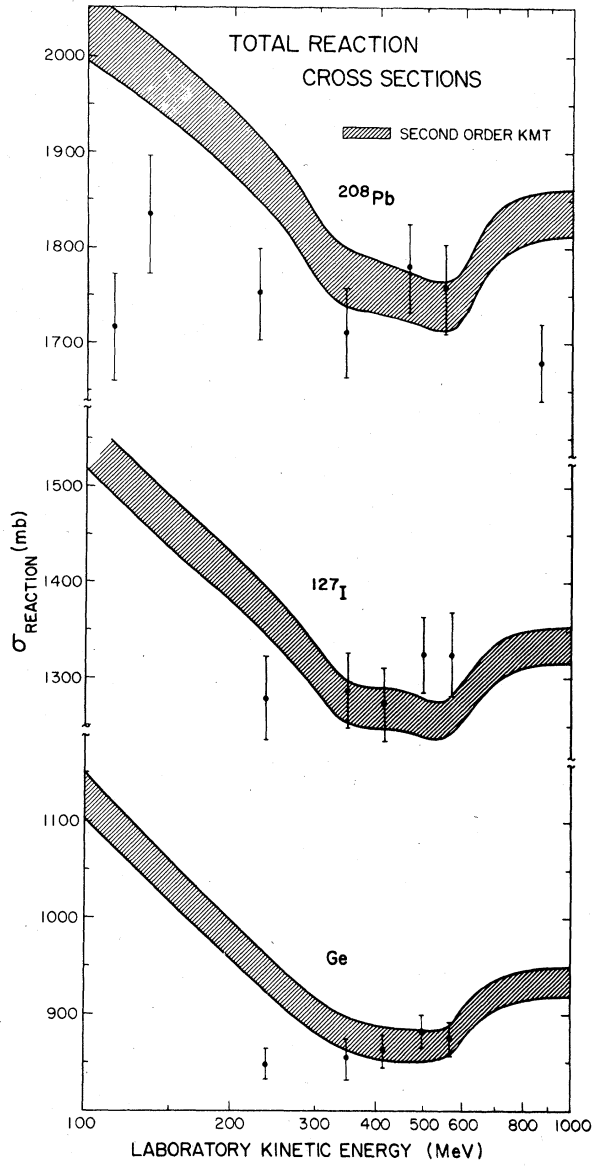

FIG. 5. Same as Fig. 4 except for Ge, ^{127}I, and ^{208}Pb.

certainty in the theoretical predictions. Generally the size of the error bars and the magnitude of the scatter of the data displayed in Figs. 4 and 5 are much larger than the uncertainty in the corresponding theoretical predictions and improved data, especially in the 700 to 2200 MeV region, would be quite useful.

The overestimate by the impulse approximation prediction at low energies is not unexpected, based on several theoretical arguments. Nonlocal corrections by Mulligan[51] and Johnson and Martin,[52] off-shell effects as studied by Scheerbaum *et al.*,[60] Pauli reduction of the free N-N scattering amplitude as estimated by Clementel and Villi,[61] and avoiding the closure approximation in the first-order potential as discussed by Tandy *et al.*[62] are some of the additional corrections to be found in the literature. All of these theoretical improvements tend to reduce the impulse approximation result for total cross sections, particularly at lower energies.

Recently, Ernst[20] has calculated proton-nucleus total reaction cross sections from 100 MeV to 1 GeV using the impulse approximation and the optical limit of Glauber theory[12] and has obtained fairly good reproduction of the data over this en-

tire range, in disagreement with the results given here. In calculating σ_{REAC}, Ernst makes two serious oversimplifications. First, in using the optical limit of Glauber theory, the dependence of σ_{REAC} on the real part of the optical potential is omitted, thus causing the computed values to be about 8% too low at low energies. Second, the range of the spin-independent N-N scattering amplitude, B_{pj}, is assumed to be constant from 100 to 1000 MeV, although Table I demonstrates that an order of magnitude variation occurs throughout this energy range. Ernst's assumption of a constant B_{pj}, which he evaluates at ~1 GeV, results in another ~10% underestimate of the reaction cross section at low energies. Thus the total reaction cross sections computed in Ref. 20 are quite inaccurate at low energies (~100 to 400 MeV) and the results given here, although being in worse agreement with experiment, much better represent the impulse approximation prediction than the calculations of Ref. 20.

In the energy range above 400 MeV the agreement with the data is very good (except with the 860 MeV σ_{REAC} data from Ref. 18). In this energy regime the ratio of $\sigma_{TOTAL(REAC)}$ (theory) to $\sigma_{TOTAL(REAC)}$ (exp) has been computed for each data point (except for the 860 MeV data of Ref. 18) and the average of all these values computed. The resulting average ratio is 1.025. Also at each data point the theoretical and experimental errors have been quadratically added and the average of all these errors computed. The average combined theoretical and experimental error is ±3.8% in the 400 to 2200 MeV range. Hence, on the average above 400 MeV, the predicted and the experimental total and reaction cross sections differ by less than one standard deviation in the average of the combined experimental and theoretical uncertainties. Considering that most of the predictions shown in Figs. 3–5 do not rely on complementary elastic angular distribution data, the predictive ability of the optical potential in Eq. (32) is quite impressive, at least above 400 MeV. What this means is that one should expect to obtain excellent quality fits to elastic scattering data using Eq. (32) at energies greater than 400 MeV. The fit quality should be comparable to that seen already at 800 and 1000 MeV.[1-10] Below 400 MeV the ability to accurately describe elastic scattering with Eq. (32) should begin to deteriorate if one is allowed to vary only the geometry of the neutron density. This statement has been partially confirmed by recent calculations using the first-order KMT optical potential and the impulse approximation for proton elastic scattering at 135 and 182 MeV on ^{90}Zr and ^{208}Pb.[63] These calculations use the same proton and neutron densities as employed at 800 MeV,[2,3] and although the positions of the diffractive maxima and minima are correctly reproduced as is the overall slope of the angular distribution, the fits are not of comparable quality to that obtained at ~1 GeV.[1-10] The ~150 MeV predicted cross sections tend to have minima which are too deep and fail to carefully reproduce details of the back angle diffractive structure. Such discrepancies should be symptomatic of any impulse calculation below 400 MeV based on the results seen here for σ_{TOTAL} and σ_{REAC}.

In Fig. 6 the effects of the second-order optical potential terms on σ_{TOTAL} for ^{16}O and σ_{REAC} for ^{208}Pb are indicated. Calculations which include correlations are indicated by the solid lines and those omitting correlation corrections are shown as the dashed curves. The general effect of the correlation terms is to increase the absorption, thus raising

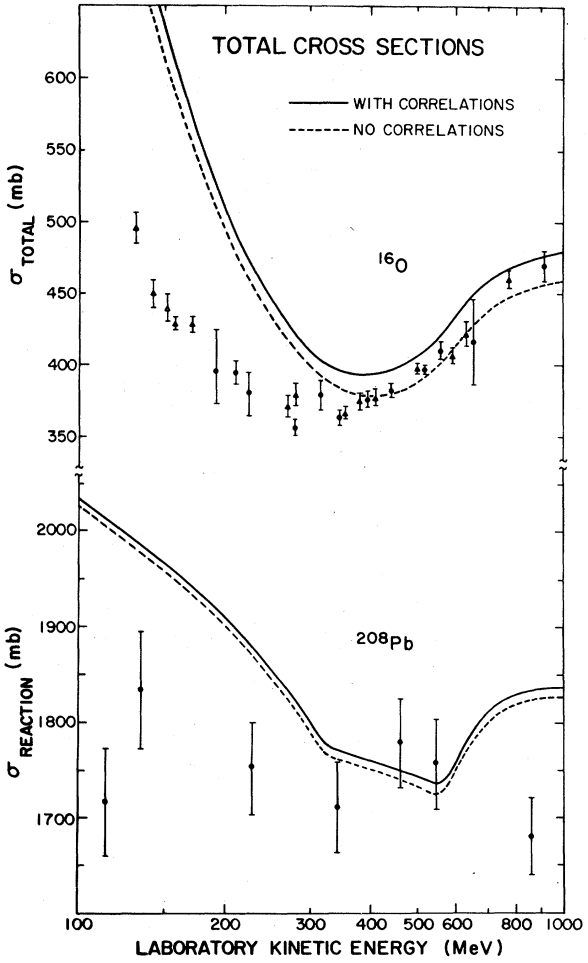

FIG. 6. Proton-nucleus total cross sections for ^{16}O and total reaction cross sections for ^{208}Pb computed with (solid curves) and without (dashed curves) the correlation corrections discussed in the text.

σ_{TOTAL} and σ_{REAC} by about 4% in ^{16}O and 1% in ^{208}Pb. The reader is reminded of the fact that the local approximations used here for the second-order terms of the optical potential probably do not accurately represent the full, nonlocal second-order potential at low energies as is pointed out by Johnson and Martin.[52] The calculations of Ref. 52 demonstrate that below 300 MeV the addition of nonlocal second-order terms causes the total reaction cross sections to decrease.

The obvious conclusion to be drawn from Figs. 3–6 is that the kind of second-order KMT calculation embodied in Eq. (32) and as applied to proton elastic scattering at 800 and 1000 MeV will not be adequate below 400 MeV. Whether this breakdown is due to some inadequacy of the KMT formalism or of the impulse approximation or if it is due to some omitted correction which becomes significant below 400 MeV will need to be resolved before attempting KMT analyses of proton-nucleus scattering at these lower energies. Some possible, additional corrections not included here which one would expect to become more significant at lower energies are listed here. Projectile-target antisymmetrization,[61,64] virtual charge exchange,[6] Fermi motion averaging,[65,66] binding energy corrections,[11] and other nonlocality or off-shell effects[11,51,52,60,62] can be expected to become more significant at these lower energies.

As an example of the kind of effect that two of these corrections could have at energies below 300 MeV, the Pauli reduction of σ_{pj}^{T} as estimated by Clementel and Villi[60,61] and the first-order KMT optical potential nonlocality correction estimate of Mulligan[51] have been applied to the cases of ^{16}O, ^{63}Cu, and ^{208}Pb. The results are shown in Fig. 7. The solid curves are the impulse approximation results (without error bands) as given previously in Figs. 3–5 while the dashed curves include only the Mulligan[51] nonlocality correction and the dash-dot curves include both the Mulligan correction as well as the Clementel and Villi[61] Pauli reduction effect. Both estimates provide overall reduction factors for the well depths of the real and imaginary parts of the first-order, $t(q)\bar{\rho}(q)$ optical potential. In the latter calculation both of the reduction factors were multiplied together to give the combined result shown in Fig. 7. The Clementel and Villi correction was assumed to reduce only the imaginary part of the optical potential as in Ref. 60. Clearly, this simple method of combining these two corrections is very crude, as are the correction estimates in Refs. 51 and 61 themselves. The curves in Fig. 7 are merely intended to qualitatively indicate the direction and order of magnitude that these two higher order corrections have at low energies. The results

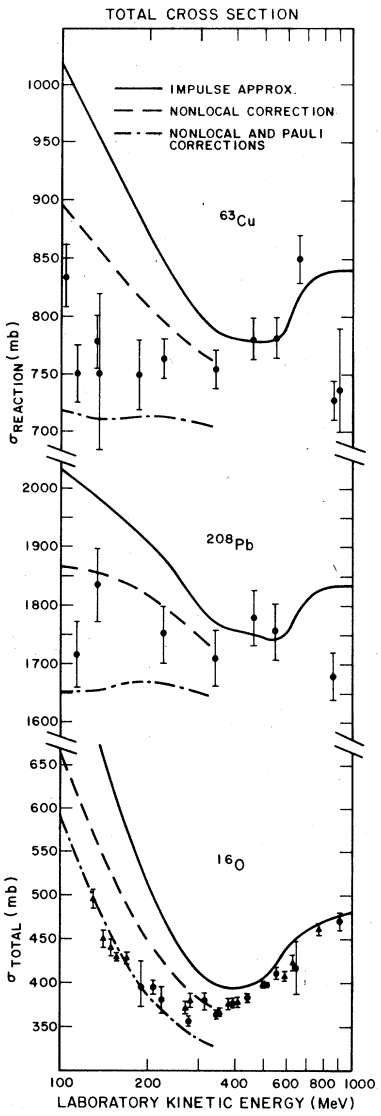

FIG. 7. Theoretical KMT predictions of σ_{TOTAL} and σ_{REAC} for p + ^{16}O, ^{63}Cu, and ^{208}Pb using the impulse approximation (solid curves), the nonlocality correction of Mulligan (Ref. 51) (dashed curves), and both the Mulligan correction and the Pauli reduction factor of Clementel and Villi (Ref. 61) (dash-dot curves). The dashed and dash-dot curves do not extend above 325 MeV because of the limited energy range assumed in Ref. 51.

shown in Fig. 7 should encourage a careful attempt to extend KMT calculations to these lower energies, below 400 MeV, and should warn analysts against making unjustifiable assumptions in this energy range.[20]

Glauber model calculations of σ_{TOTAL} for ^{12}C and ^{16}O by Schwaller *et al.*[13] and by Ahmad and Khan[67] in which an α-cluster model for ^{12}C and ^{16}O are assumed and in which proton-alpha scattering amplitudes constitute the fundamental in-

teraction give good overall agreement with the σ_{TOTAL} data for these nuclei from 150–1000 MeV. These calculations suggest that the multiple scattering formalism is sufficient but that some additional many-body corrections, including those discussed above, which the p-α amplitude empirically contains is needed in the standard multiple scattering calculation which relies on free N-N scattering amplitudes.

To close this section a discussion of the usefulness of σ_{TOTAL} and σ_{REAC} as a direct measure of neutron radii will be given. Such an analysis is presented in the recent work of Ernst.[20] To begin, consider the following hypothetical example. Suppose one were to perform the above second-order KMT calculation of σ_{TOTAL} and σ_{REAC} and fit the corresponding data by varying the neutron matter distribution. From Figs. 3–5 and Table III one can immediately see that differences of about 1–2 fm in $\langle r_n^2\rangle^{1/2}$ would result from fitting the available data from 100–2200 MeV. The recent ~150 MeV impulse approximation calculations mentioned earlier[63] use the same proton and neutron densities as obtained from analyses of the 0.8 GeV proton scattering data[2,3] and as stated before are in fairly good agreement with the ~150 MeV data with respect to maxima-minima positions and the overall slope of the diffractive pattern. Clearly the deduced neutron densities which result in optimal fits to the elastic differential cross section will not vary nearly so radically with energy as would those which result from direct fits to the total or reaction cross section data. Variations in $\langle r_n^2\rangle^{1/2}$ of about $\lesssim$0.1 fm between fits to $d\sigma/d\Omega$ at ~150 and ~1000 MeV should result compared to variations of 1–2 fm for the direct fitting of σ_{TOTAL} and σ_{REAC}.

If one now attempts to fit σ_{TOTAL} and σ_{REAC} at higher energies, say 1 GeV, where the predicted and experimental total cross sections agree to within 2.5%, one finds that a change in $\langle r_n^2\rangle^{1/2}$ of about 0.2 fm is required in order to remove this 2.5% discrepancy for any nucleus with $12 \leq A \leq 208$. Suppose however that some additional theoretical correction was found which would remove this 2.5% discrepancy. Applying this same hypothetical correction to the σ_{TOTAL} calculation would change the result for $\langle r_n^2\rangle^{1/2}$ by 0.2 fm. Suppose also that after including this new correction term the fit to the elastic angular distribution was recovered by varying $\rho_n(r)$ and for simplicity assume that this hypothetical correction had the effect of altering the overall strength of the imaginary potential (i.e., change the effective value of σ_{pj}^T as in the correction estimates of Refs. 51 and 61). From the error analyses of Refs. 3 and 44 it is known that a change in σ_{pj}^T which is sufficient to produce a 2.5% change in σ_{TOTAL} will result in a 0.015 to 0.07 fm change in $\langle r_n^2\rangle^{1/2}$ for ^{16}O and ^{208}Pb, respectively, when the fit to the elastic angular distribution is recovered.

The point of these examples is to demonstrate that using σ_{TOTAL} and σ_{REAC} to determine neutron radii is roughly *an order of magnitude worse* technique than determinations based on analyses of differential cross sections. As has been explained, the deduced neutron radii resulting from analyses of angular distributions at widely variant energies are remarkably stable. However, determinations of neutron radii by fitting total cross sections directly would result in a large and very erratic energy dependence. Furthermore, angular distribution determinations of $\langle r_n^2\rangle^{1/2}$ in the ~1 GeV region should be stable with respect to theoretical improvements, as seen explicitly for example when correlation terms are added to the calculations.[4,9] On the other hand, total cross section determinations of $\langle r_n^2\rangle^{1/2}$ would be very sensitive to theoretical improvements. Clearly one should not consider proton-nucleus total cross sections as accurate measures of neutron matter radii. Furthermore, analysts *cannot* require the deduced neutron densities to fit both the total cross sections and angular distributions in their analyses since, in general, totally different densities would be required by the optical potential formalism embodied in Eq. (32). From the above discussion it is clear that the angular distribution determined densities are more reliable. Only if one were to have available a physically "exact" theory could such a dual requirement be properly imposed on the analysis.

IV. SUMMARY AND CONCLUSIONS

The primary results of the calculations presented here are: (1) that the standard application of the Kerman, McManus, and Thaler optical potential formalism contained in Eq. (32) of Sec. II satisfactorily predicts the total and reaction cross sections for a wide range of nuclei at energies greater than ~400 MeV (to within about 3%), and (2) the same calculation (Eq. 32) fails to correctly predict σ_{TOTAL} and σ_{REAC} below 400 MeV, the degree of failure being about a 15–25% overestimate of the total and reaction cross section strengths. Since these theoretical σ_{TOTAL} and σ_{REAC} are *absolute predictions* (within the given error band), the test imposed on the KMT calculation here is in lowest order an absolute accuracy measure of the theory and its application. The test is considered lowest order since σ_{TOTAL} and σ_{REAC} are primarily determined by σ_{pj}^T and are not too strongly dependent on the other N-N amplitudes or to details of the momentum transfer dependence of

the spin-independent N-N amplitude.

The application of KMT theory to proton scattering at energies below 400 MeV will require careful investigation of a number of additional corrections which could become important as the incident energy is reduced. Projectile-target antisymmetrization, virtual charge exchange, Fermi motion averaging, binding energy corrections, and nonlocal or off-shell effects were suggested as possible additional corrections to consider at these lower energies. Simple estimates of two of these corrections were taken from the literature[51,61] and applied to several of the cases studied here.

The usefulness of total and reaction cross sections in determining neutron densities was discussed. It was explained that erratic energy dependence and extreme sensitivity to experimental errors and theoretical improvements would be an inevitable feature of neutron densities which have been determined in this way. The conclusion is that neutron densities are best investigated by analyses of elastic differential cross section data. Because of the approximate nature of any numerical application of a many-body scattering theory in which theoretical uncertainties will always persist, one should study matter distributions by analyzing the angular distribution data independently from and not in conjunction with σ_{TOTAL} and σ_{REAC} data.

This test of KMT theory's ability to accurately predict σ_{TOTAL} and σ_{REAC} is not a final, definitive test of the absolute accuracy of the KMT theory, nor is the apparent success above 400 MeV an indication that no problems with the theory or its application exist in this energy region. The success in this energy regime indicates that at least no serious, lowest order problems with the standard application of KMT theory exist above 400 MeV.

ACKNOWLEDGMENTS

The author would like to thank Professor E. Lomon for helpful discussions regarding the N-N phase shifts and Dr. Gary Blanpied for carefully reading the manuscript. This research was supported in part by the United States Department of Energy.

[1]G. W. Hoffmann *et al.*, Phys. Lett. 76B, 383 (1978) and 79B, 376 (1978).
[2]L. Ray, G. W. Hoffmann, G. Blanpied, W. R. Coker, and R. P. Liljestrand, Phys. Rev. C 18, 1756 (1978).
[3]L. Ray, W. R. Coker, and G. W. Hoffmann, Phys. Rev. C 18, 2641 (1978).
[4]L. Ray, Phys. Rev. C 19, 1855 (1979).
[5]G. K. Varma and L. Zamick, Nucl. Phys. A306, 343 (1978).
[6]D. R. Harrington and G. K. Varma, Nucl. Phys. A306, 477 (1978).
[7]E. Boridy and H. Feshbach, Ann. Phys. (N. Y.) 109, 468 (1977).
[8]V. Layly and R. Schaeffer, Phys. Rev. C 17, 1145 (1978).
[9]A. Chaumeaux, V. Layly, and R. Schaeffer, Ann. Phys. (N. Y.) 116, 247 (1978).
[10]G. D. Alkhazov, S. L. Belostotsky, and A. A. Vorobyov, Phys. Rep. 42C, 89 (1978), and references therein.
[11]A. K. Kerman, H. McManus, and R. M. Thaler, Ann. Phys. (N. Y.) 8, 551 (1959).
[12]R. J. Glauber, in *Lectures in Theoretical Physics*, edited by W. E. Brittin and L. G. Dunham (Interscience, New York, 1959), p. 315; see also *High Energy Physics and Nuclear Structure*, edited by G. Alexander (North-Holland, Amsterdam, 1967), p. 311 and *High Energy Physics and Nuclear Structure*, edited by S. Devons (Plenum, New York, 1970), p. 207.
[13]P. Schwaller *et al.*, CERN Technical Report No. CERN 72-13, 1972; Nucl. Phys. A316, 317 (1979) and references therein.
[14]P. U. Renberg *et al.*, Nucl. Phys. A183, 81 (1972).
[15]A. Johansson, U. Svanberg, and O. Sundberg, Ark. Fys. 19, 527 (1961).
[16]J. M. Cassels and J. D. Lawson, Proc. Phys. Soc. (London) 67, 125 (1954).
[17]R. Goloskie and K. Strauch, Nucl. Phys. 29, 474 (1962).
[18]F. F. Chen, C. P. Leavitt, and A. M. Shapiro, Phys. Rev. 99, 857 (1955).
[19]V. Franco, Phys. Rev. C 6, 748 (1972).
[20]D. J. Ernst, Phys. Rev. C 19, 896 (1979) and B. D. Anderson *et al.*, Phys. Rev. C 19, 905 (1979).
[21]H. Feshbach, A. Gal, and J. Hüfner, Ann. Phys. (N. Y.) 66, 20 (1971).
[22]J. J. Ullo and H. Feshbach, Ann. Phys. (N. Y.) 82, 156 (1974).
[23]R. A. Arndt, R. H. Hackman, and L. D. Roper, Phys. Rev. C 9, 555 (1974); 15, 1002 (1977).
[24]M. J. Moravcsik, *The Two-Nucleon Interaction* (Clarendon, Oxford, 1963), pp. 11–18.
[25]M. H. MacGregor, M. J. Moravcsik, and H. P. Stapp, Annu. Rev. Nucl. Sci. 10, 291 (1960).
[26]H. P. Stapp, T. J. Ypsilantis, and N. Metropolis, Phys. Rev. 105, 302 (1957).
[27]E. Lambert and H. Feshbach, Ann. Phys. (N. Y.) 76, 80 (1973).
[28]J. Bystricky, F. Lehar, and Z. Janout, Report No. CEA-N-1547 (E)-Saclay-Août (1972).
[29]O. Benary, L. R. Price, and G. Alexander, Report No. UCRL-20000NN Lawrence Berkeley Laboratory, 1970 (unpublished).
[30]T. J. Devlin *et al.*, Phys. Rev. D 8, 136 (1973).
[31]A. A. Vorobyov *et al.*, Phys. Lett. 41B, 639 (1972).
[32]O. V. Dumbrais, Yad. Fiz. 13, 1096 (1971) [Sov. J. Nucl.

Phys. 13, 626 (1971)].
[33]G. J. Igo, Rev. Mod. Phys. 50, 523 (1978).
[34]W. Grein and P. Kroll (unpublished).
[35]A. A. Carter and D. V. Bugg, Phys. Lett. 20, 203 (1966).
[36]H. B. Willard *et al.*, Phys. Rev. C 14, 1545 (1976).
[37]P. R. Bevington *et al.*, Phys. Rev. Lett. 41, 384 (1978).
[38]R. Carlini *et al.*, Phys. Rev. Lett. 41, 1341 (1978).
[39]V. P. Dzhelepov, B. M. Golovin, V. S. Nadezhdin, and V. I. Satarov, in *Proceedings of the Twelfth International Conference on High Energy Physics, Dubna, 1964* edited by Ya. A. Smorodinskii *et al.* (Atomizdat, Moscow, 1966), Vol. 1, p. 11.
[40]M. L. Marshak *et al.*, Phys. Rev. C 18, 331 (1978).
[41]I. Sick and J. S. McCarthy, Nucl. Phys. A150, 631 (1970).
[42]C. W. de Jager, H. de Vries, and C. de Vries, At. Data Nucl. Data Tables 14, 479 (1974).
[43]B. Frois *et al.*, Phys. Rev. Lett. 38, 152 (1977).
[44]G. Adams *et al.*, Phys. Rev. Lett. 43, 421 (1979).
[45]J. W. Negele and D. Vautherin, Phys. Rev. C 5, 1472 (1972); the DME code of Negele provided the numerical results given here.
[46]P. L. Roberson, D. A. Goldberg, N. S. Wall, L. W. Woo, and H. L. Chen, Phys. Rev. Lett. 42, 54 (1979).
[47]W. Bertozzi, J. Friar, J. Heisenberg, and J. W. Negele, Phys. Lett. 41B, 408 (1972).
[48]G. Höhler *et al.*, Nucl. Phys. B114, 505 (1976).
[49]T. Tamura, W. R. Coker, and F. Rybicki, Comput. Phys. Commun. 2, 94 (1971).
[50]E. Kujawski and J. P. Vary, Phys. Rev. C 12, 1271 (1975).
[51]B. Mulligan, Ann. Phys. (N. Y.) 26, 159 (1964).
[52]R. C. Johnson and D. C. Martin, Nucl. Phys. A192, 496 (1972).
[53]A. de Shalit and H. Feshbach, *Theoretical Nuclear Physics* (Wiley, New York, 1974), pp. 135–140.
[54]M. D. Cooper and M. B. Johnson, Nucl. Phys. A260, 352 (1976).
[55]M. L. Goldberger and K. M. Watson, *Collision Theory* (Wiley, New York, 1964).
[56]B. R. Martin, *Statistics for Physicists* (Academic, London, 1971), pp. 85–93.
[57]G. Igo *et al.*, Phys. Lett. 81B, 151 (1979).
[58]G. Igo and G. W. Hoffmann, private communication.
[59]G. S. Blanpied *et al.*, Phys. Rev. C 18, 1436 (1978), and Phys. Rev. C (to be published).
[60]R. R. Scheerbaum, C. M. Shakin, and R. M. Thaler, Phys. Rev. C 7, 2346 (1973).
[61]E. Clementel and C. Villi, Nuovo Cimento 2, 176 (1955).
[62]P. C. Tandy, E. F. Redish, and D. Bollé, Phys. Rev. C 16, 1924 (1977).
[63]P. Schwandt, F. Petrovich, and A. Picklesimer, private communication.
[64]R. R. Scheerbaum, Phys. Rev. C 7, 2166 (1973).
[65]S. J. Wallace, Phys. Rev. C 12, 179 (1975).
[66]L. Ray and W. R. Coker, Phys. Rev. C 16, 340 (1977).
[67]I. Ahmad and Z. A. Khan, Nucl. Phys. A274, 519 (1976).